Supplemental Information: Condensation Diffusion Charging - Particle Number Measurement of High Concentrations Down to 2.5 nm

Helmut Krasa[1], Victoria M. Fruhmann[1], Sebastian Schurl[2], Martin Kupper[1], and Alexander Bergmann[1]

[1]Institute of Electrical Measurement and Sensor Systems, Graz University of Technology, Graz, Austria
[2]Institute of Thermodynamics and Sustainable Propulsion Systems, Graz University of Technology, Graz, Austria

Correspondence: Alexander Bergmann (alexander.bergmann@tugraz.at)

Particle growth analysis

Equations governing the particle growth rate are discussed in further detail in this section.

Following particle activation, the droplet grows along its trajectory at the following rate:

$$\frac{d\,d_p}{dt} = \frac{4D\nu_m\chi}{RT} \cdot \frac{p - p_p}{d_p} \tag{S1}$$

D is the diffusion coefficient, and χ is the correction factor outside the continuum regime. p_p is the equilibrium vapor pressure at the droplet surface of the surrounding gas with the pressure p at the current particle position. With the Fuchs-Sutugin approach (Davis, 1982), the value of χ is given as:

$$\chi = \frac{1 + Kn}{1 + 1.71Kn + 1.333Kn^2} \tag{S2}$$

Kn is the Knudsen number $Kn = 2\lambda/d_p$. λ is the mean free path of molecules in the air. The vapor pressure at the droplet surface is:

$$p_p = p_s(T_p)\exp\left(\frac{4\sigma v_m}{RT_p d_p}\right) \tag{S3}$$

p_s is the saturation vapor pressure of the WF. T_p is the temperature at the droplet surface and changes due to condensation on the droplet surface and is therefore dependent on the condensation rate $d\,d_p/dt$:

$$\frac{d\,T_p}{dt} = \frac{3}{c_p\rho d_p}\left(H_{vap}\rho\frac{d\,d_p}{dt} - 4k_g\frac{(T_p - T)\chi_h}{d_p}\right) \tag{S4}$$

The material parameters of the WF are the heat capacity c_p, density ρ, the latent heat of vaporization H_{vap} and the thermal conductivity of the surrounding gas k_g. χ_h corrects for heat transfer outside of the continuum regime.

The first term describes the latent heat added due to condensation resulting from the phase change of the WF from gaseous to fluid. The second term describes the heat flux of the hotter droplet towards the surrounding gas. χ_h is calculated as follows:

$$\chi_h = \left(1 + \frac{2k_g}{\alpha_t d_p \rho_g c_{pg}}\sqrt{\frac{2\pi m_g}{RT}}\right)^{-1} \tag{S5}$$

The subscript g indicates the material parameters of the surrounding gas. m_g, ρ_g and c_{pg} are the average molecular mass, density and heat capacity, respectively. The thermal accommodation coefficient α_t was assumed to be one according o Seinfeld and Pandis (2016), which give a more in-depth description of the particle growth rate.

Saturation profile and particle activation

Simulated supersaturation, vapor concentration and particle activation data are shown. Furthermore, particle activation at a temperature setting of T_c = 40 °C and T_S = 20°C was evaluated experimentally.

The supersaturation profile shows a higher peak supersaturation for a larger ΔT, whereas as total vapor concentration and therefore particle growth rate, is mainly determined by the saturator temperature T_S.

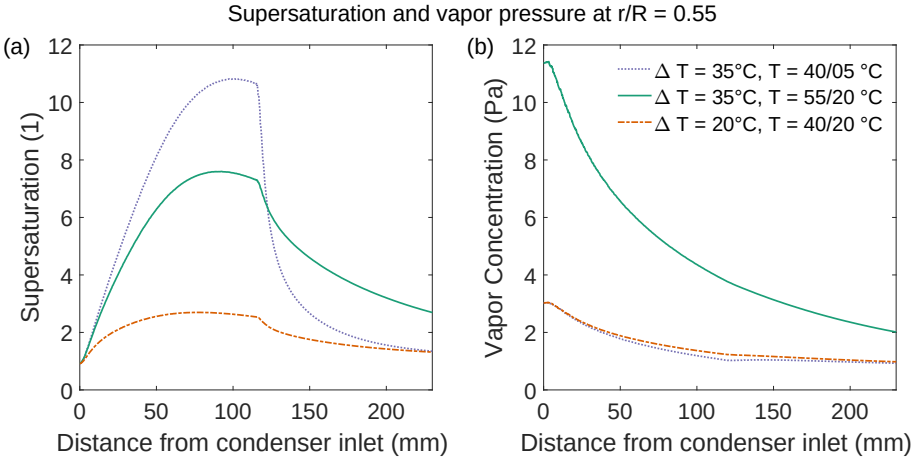

Figure S1. (a) Supersaturation and (b) vapor concentration profile along the growth axis for the three modeled temperature settings .

The simulated supersaturation profile and particle activation closely correlate and show, as expected, a maximum supersaturation at the center of the condenser. Particle sizes within the transition zone of the CPC (CE < 1) only activate up to a certain distance from the centerline of the condenser.

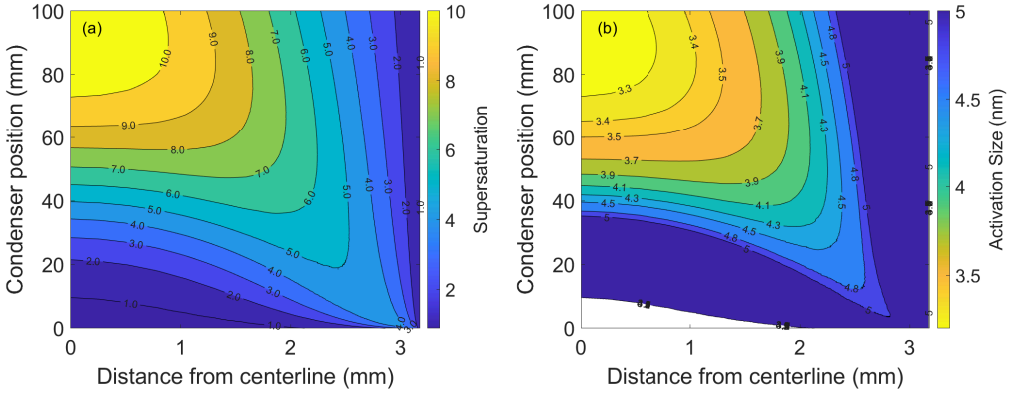

Figure S2. Contour plots of the (a) supersaturation field and (b) equilibrium Kelvin diameter of the condenser at a temperature setting of $T_s = 55$ °C and $T_c = 20$ °C

The particle activation efficiency of the condensation stage at a reduced saturator/condenser temperature of $T = 40/20$°C with DEG shows a good agreement with results obtained by the simulation. Particle counting was performed using a 23 nm CPC used as detection unit. The CPC was evaluated prior without the condensation stage prior and was found to have a d_0 value of 14 nm with Ag particles and was therefore suitable to evaluate the activation efficiency of the condensation stage without characterizing the CE of the charger.

The fitted d_{50} activation diameter was determined to be 9.5 nm. This value lies between the theoretical predictions from heterogeneous nucleation theory: 7 nm for perfect wetting conditions ($\theta = 0°$) and 10.2 nm for a contact angle of $\theta = 20°$.

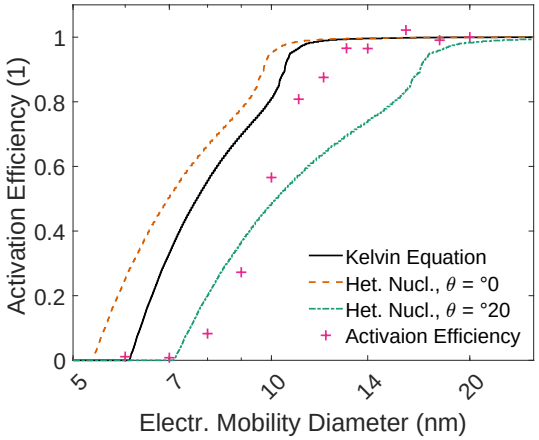

Figure S3. Activated particle sizes of the condensation stage at a temperature setting of $T_c = 40$ °C and $T_s = 20$ °C with Ag aerosol.

Concentration-dependent response for glycerol

Due to the lower temperature settings and and reduced vapor pressure of glycerol, the droplet size was significantly smaller and the amplification was a factor of 4 compared to 20 with DEG at the default saturator temperature of $T = 55$ °C. Furthermore, due to reduced influence of concentration-dependent effects, the droplet size is not reduced for concentrations up to $> 10^5$ cm^{-3}.

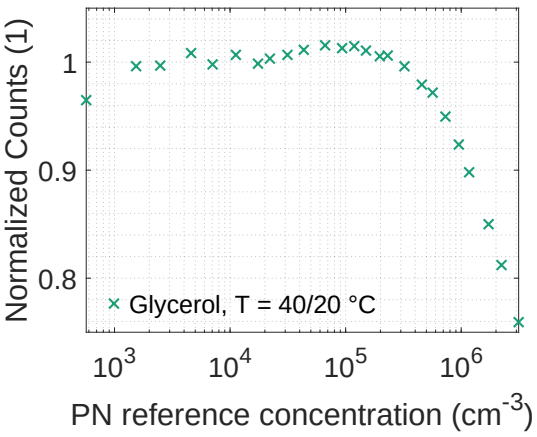

Figure S4. Linear response with glycerol as working fluid at a saturator and condenser temperature of $T = 40$ °C and $T = 20$ °C.

Chassis dynamometer measurements at high concentrations

To increase the measured PN concentration range of the CDC, the instrument was placed in the CVS tunnel measuring parallel to the sampling system instead. The PN reduction factor within the dilution system was 1:196. To stay within the concentration limits of the CDC, the sampled aerosol was diluted by a factor of 1:10. The data were recalculated to the PN concentration in the CVS tunnel. As the volatile particle remover could not be removed from the reference system, the reference system measured the solid PN concentration, while the CDC measurement included semi-volatile particles. Furthermore, to account for concentration-dependent effects of the CDC, a concentration dependent fit function obtained from the measurement points in Figure 6 was used.

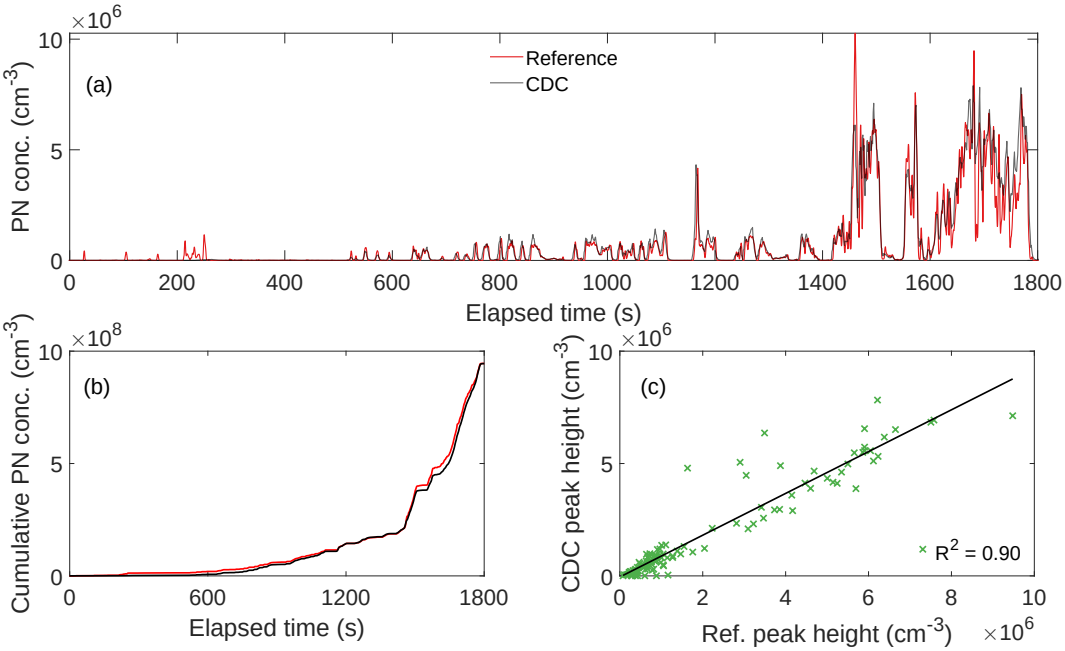

Figure S5. Calibrated results from the chassis dynamometer test. (a) Time-dependent measured concentration in the CVS tunnel of both the CDC counter and a reference counter. (b) Background-adjusted the cumulative PN concentration of both counters. (c) Correlation of detected emission peaks.

Literature:

Davis, E. J.: Transport phenomena with single aerosol particles, Aerosol Science and Technology, 2, 121–144, https://doi.org/10.1080/02786828308958618, 1982.

Seinfeld, J. H. and Pandis, S. N.: Atmospheric Chemistry and Physics: From Air Pollution to Climate Change, Wiley-VCH, New York, 3rd edn., ISBN 978-1-118-94740-1, 2016.